Unusual Compression Behavior of Anatase TiO_2 Nanocrystals

Varghese Swamy,[1,*] Alexei Y. Kuznetsov,[2] Leonid S. Dubrovinsky,[3] Alexander Kurnosov,[3] and Vitali B. Prakapenka[4]

[1]*Department of Materials Engineering, Monash University, Victoria 3800, Australia*
[2]*Divisão de Metrologia de Materiais (DIMAT), Inmetro, Duque de Caxias, Rio de Janeiro, Brazil*
[3]*Bayerisches Geoinstitut, University of Bayreuth, D-95440 Bayreuth, Germany*
[4]*The Consortium for Advanced Radiation Sources, University of Chicago, Chicago, Illinois 60637, USA*

(Received 17 April 2009; published 13 August 2009)

The size-dependent stiffness variations in nanocrystalline anatase, a leading material for applications in photovoltaics, photocatalysis, photoelectrochromics, sensors, and optical coatings, were determined using *in situ* synchrotron x-ray diffraction and Raman scattering. An unusual, abrupt change in the compression curve at ~10 GPa and subtle breaks in the pressure shifts of the intense E_g Raman band at ~10 and ~15 GPa have been correlated with ~2 Å-scale disordering of nanocrystalline anatase structure that fully amorphizes under high compression.

DOI: 10.1103/PhysRevLett.103.075505 PACS numbers: 62.25.−g, 61.46.Df, 62.50.−p, 64.70.Nd

The promise of size-tailored mechanical properties in nanoscale materials and their applications has been driving intense research aimed at characterizing the nanomechanical behaviors of materials. One way to experimentally investigate the nanomechanical behaviors (including elastic and nonelastic deformations and potential phase transitions), although not completely unambiguous, is to employ the nanoindentation-based local probes [1]. A complementary experimental approach, that adopted in the present study, is to investigate systematically the size dependence of the mechanical properties using well characterized, size-controlled nanoscale samples *in situ* under specific stress (pressure)-temperature regimes. The latter approach allows for the direct characterization of the mechanical properties such as stiffness and the average atomic-level structures contributing to specific modifications to these properties under nanometric size regimes. Here we report an investigation of the compression behavior of nanocrystalline (nc) anatase TiO_2 under hydrostatic or quasihydrostatic conditions and ambient temperature using the diamond-anvil cell (DAC) technique. We correlate the unusual compression behavior observed for nc anatase with intracrystallite atomic-level structural reorganizations.

Nanoscale TiO_2 phases, especially anatase and rutile, are among the most promising materials for a wide range of advanced technological applications. While much of the current attention on TiO_2 is focused on applications based on the exceptional photoactivity of nanoscale anatase and rutile (dye-sensitized solar cells, photocatalysts, environmental decontamination, etc.) [2,3], there are other applications where the nanomechanical properties of titania could potentially be significant to the material's performance. The use of TiO_2 in optical coatings, based on the outstanding optical properties (excellent hydrophilicity in the case of anatase) [4], is an example. TiO_2 could also serve as an excellent model for the study of the relatively poorly understood nanomechanical behaviors of ceramic systems. In fact, nc-rutile TiO_2 was one of the early nanoceramic systems to be investigated from a mechanical properties point of view [5].

The potential for adaptable modifications to the compression behavior of anatase in response to size, shape, or chemistry tuning has been reported [6–10]. The present work focuses on the size-dependent compression behavior of sol-gel nc anatase [11] in order to form a basis for further investigations of morphology and chemistry dependencies of the compression behaviors of nanoscale TiO_2.

We investigated nc anatase with average crystallite sizes of 6.0 ± 1 and 11.4 ± 1.2 nm (Fig. 1) with a combination of angle-dispersive synchrotron x-ray diffractometry (XRD) and Raman scattering [12]. Full XRD spectrum fitting was carried out with the convolution-based method

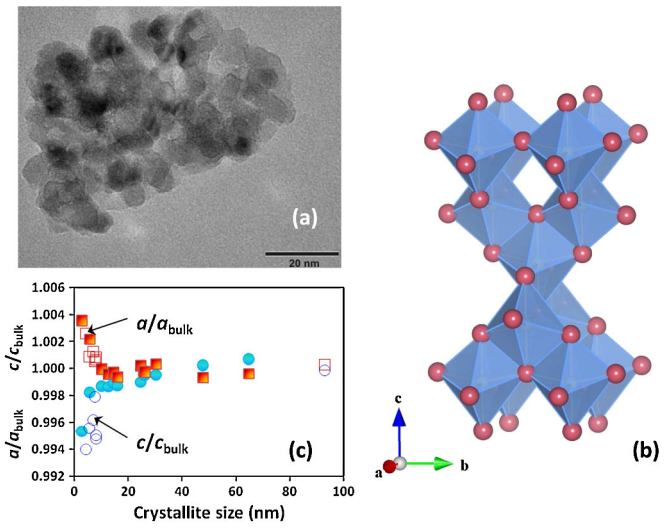

FIG. 1 (color online). (a) TEM image of 6 nm nc anatase showing crystallites with irregular morphology. (b) Polyhedral representation of the anatase structure. (c) Size-dependent variations of the anatase unit cell constants relative to bulk values. Solid symbols—Ref. [11]; open symbols—Ref. [22].

[13] implemented in TOPAS-ACADEMIC [14]. The equation of state of Au [15] (XRD) or the ruby fluorescence shift [16] (Raman) was used for pressure calibrations. A 16:3:1 methanol-ethanol-water mixture (by volume) constituted the pressure-transmitting medium in the XRD experiment and NaCl in the Raman experiments. The alcohol mixture (±water) and NaCl pressure media are typically used in high-pressure studies, including that of nanomaterials (e.g., Refs. [10,17]) and bulk oxides (e.g., Refs. [18,19]).

The anatase structure (space group $I4_1/amd$) is made up of distorted TiO_6 octahedra with four shared edges (Fig. 1). In spite of this very high degree of TiO_6 octahedral condensation (four shared edges), anatase possesses the lowest density among the most common TiO_2 structures. This intriguing characteristic of anatase lattice has been attributed to the strong repulsion of highly charged Ti ions across the shared edges [20]. The Ti-Ti repulsion induces distortion in the TiO_6 octahedra, effecting structural elongation along the c direction and shortening normal to c.

For anatase particles <10 nm, an increase in a unit cell edge, a reduction in c, and a possible increase in Ti vacancies compared to bulk structure have been reported (Fig. 1) [11,21,22]. The increase of Ti vacancies in nc anatase leading to weakened Ti-Ti repulsion and more regular TiO_6 octahedra has been invoked to explain the size-dependent lattice changes for sol-gel nc anatase [20]. Hence, the 6 nm anatase investigated in detail here falls within the size-induced anisotropic lattice modification regime and allows for the examination of the influences of structural modifications and interatomic interactions on the nanomechanical behaviors.

An example of a profile-fitted nc-anatase XRD spectrum is shown in Fig. 2. The series of *in situ* high-pressure XRD spectra [Figs. 2(a) and 2(b)] displayed suggests that, while the anatase structure is retained to ~27 GPa, there is progressive broadening and intensity reduction of the reflections with increasing pressure. At the highest pressure of 27.1 GPa, the most intense (101) anatase reflection has nearly disappeared.

Figure 3 displays the variations of the refined relative unit cell parameters for the 6 nm anatase and that of the pressure standard Au to ~23 GPa; at higher pressures the XRD intensities do not permit reliable refinement. Also shown in Fig. 3 are data on single crystal [18] and microparticle anatase [23]. The pressure evolutions of the nc-anatase lattice parameters follow quantitatively similar paths to that of the bulk equivalent to ~8 GPa. The bulk anatase structure is unstable at higher pressures (transforms to TiO_2-II), whereas the nc anatase displays enhanced pressure stability [7,24]. The disappearance of the anatase XRD reflections at ~27 GPa, replaced by a few broad, diffuse features (Fig. 2), signals the culmination of progressive disordering with pressure of the nc-anatase structure leading to complete amorphization and formation of a high-density amorphous (HDA) TiO_2 [25–27].

The pressure evolutions of the nc-anatase unit cell parameters suggest an unusual, conspicuous change in the

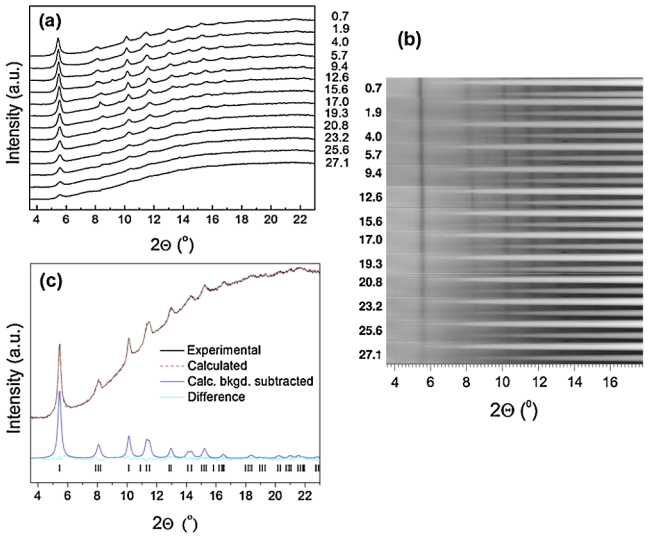

FIG. 2 (color online). (a) Integrated *in situ* XRD spectra at various pressures showing the stability of anatase structure to 27.1 GPa. (b) Spectra showing the gradual reduction in the anatase XRD intensities with pressure. (c) An example of convolution-based profile-fitted XRD spectrum of the 6 nm nc anatase (pressure = 0.7 GPa).

stiffening behavior at 10–12 GPa (Fig. 3). This abrupt change in the lattice stiffening [12], mimicking a phase transition, occurs at the pressure where the (004)-(112) and (015)-(211) pairs of d spacings cross [Fig. 4(a)]. The pressure evolution of the $d(011)$ spacing clearly illustrates the abrupt change at ~10–12 GPa [Fig. 4(b)]. The pressure dependencies of the most intense E_g Raman mode (Fig. 5) suggest nonmonotonic variations (cf. Ref. [24]), especially obvious for the coarser material, with two subtle changes at 10–12 and 14–16 GPa (Fig. 5). The different pressure dependencies of the E_g mode observed for the two samples suggest strong size-dependent responses of anatase to compression [24,25].

The anisotropic compression of bulk anatase (at $P <$ 10 GPa) with a greater linear compressibility along c than along a [18,23] is a reflection of the relative ease with which the TiO_6 octahedra shorten along c, against the Ti-Ti repulsion across the shared edges. The octahedral arrangement is inflexible (in order to maintain symmetry); the elastic responses to compression or expansion primarily reflect those of the TiO_6 octahedra [28]. The very similar compression paths for both nc anatase and bulk anatase at $P < 10$ GPa (Fig. 3), therefore, suggest very similar responses by TiO_6 octahedra in both materials to compression to 10 GPa. Nanometric dimensions do not alter the elastic nature of this compression at low pressures, as suggested by the observation that the linewidth of the most intense E_g band is recovered after pressure-cycling nc anatase in the range 0–6.2 GPa [29].

The above E_g band arises from O-Ti-O bond bending vibrations in which oxygen atoms in the TiO_6 octahedra undergo larger displacements than Ti atoms [30]; i.e., the

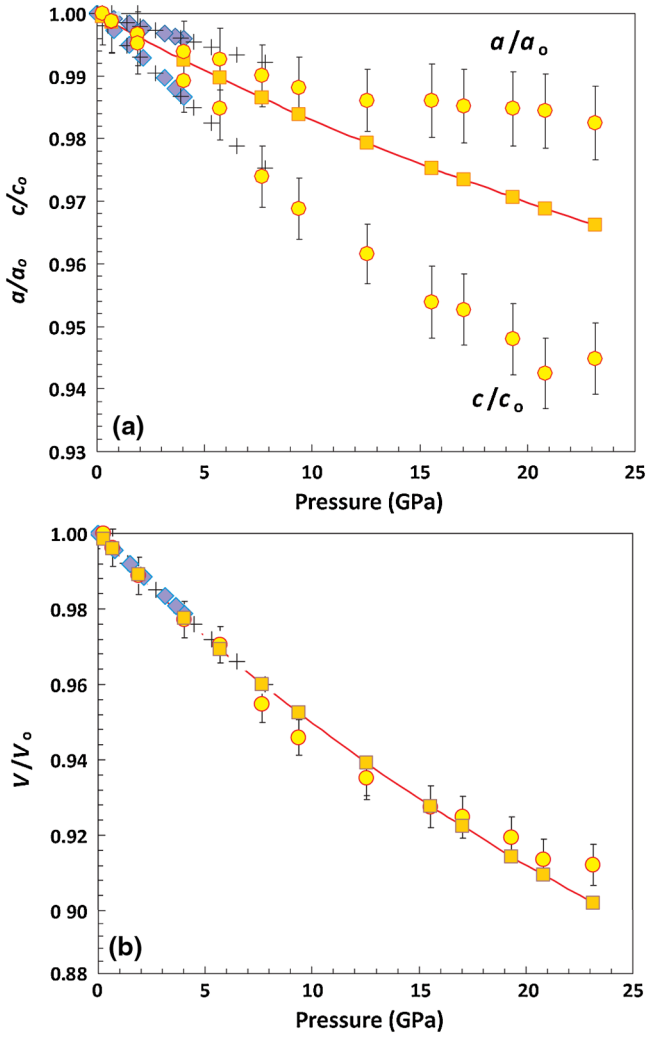

FIG. 3 (color online). The pressure-dependent variations of the relative unit cell constants. (a) a/a_o for Au (squares) and a/a_o and c/c_o for anatase (diamonds: single crystal data from Ref. [18]; plus: microparticle data from Ref. [23]; and circles: 6-nm anatase of this study). (b) V/V_o versus pressure for Au and anatase. Symbols as in (a). A clear break in the pressure evolution of the nc-anatase unit cell constants is discernible at 10–12 GPa.

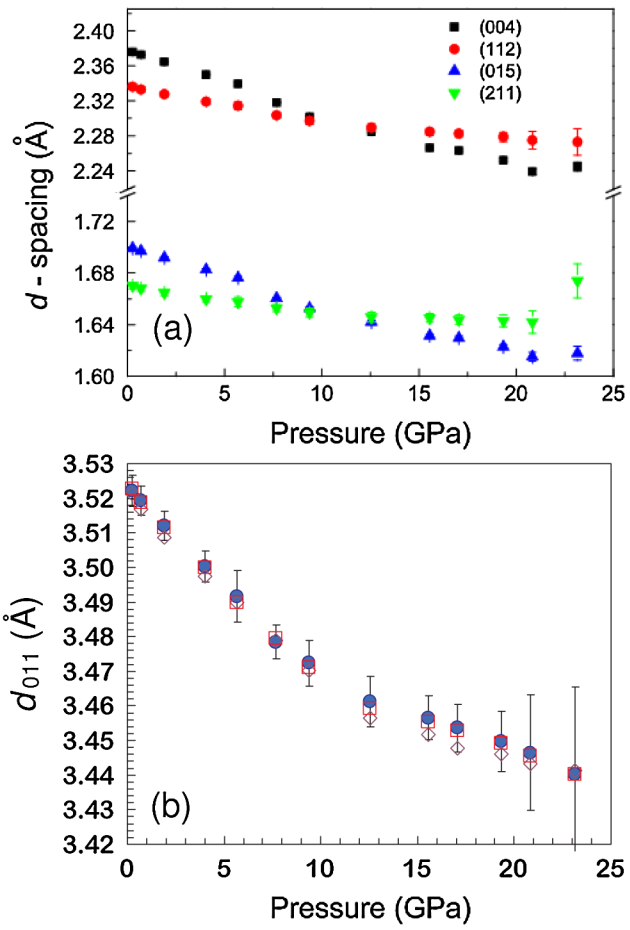

FIG. 4 (color online). (a) The pressure-dependent variations in the (004), (112), (105), and (211) d spacings. (b) Pressure vs $d(011)$ of nc anatase obtained via single-peak fit together with Au data collected near the center of the DAC (diamonds), single-peak fit (sample away from Au) (squares), and full-spectrum fit of nc-anatase XRD collected away from the DAC center (filled circles with error bars).

oxygen atoms participate more actively in the octahedral compression. Examination of deformation behavior of the anatase structure suggests that the (004) and (112) d spacings approach each other owing to the relatively larger pressure-dependent changes (shortening) in the longer apical Ti-O bonds at ~10–12 GPa. Further compression triggers destabilization of the TiO_6 octahedral arrangement. The critical-dimensioned nanocrystallinity of the material prevents its attempt to transform to the denser TiO_2-II/monoclinic-ZrO_2 structure with modified Ti-O coordination [24], and this frustrated transformation leads to local-range disordering that progressively converts the entire structure to the HDA-TiO_2 with further compression [25].

The kink in the P-V/V_o curve at 10–12 GPa (Fig. 3) indicates an abrupt increase in the stiffening of the nc-anatase structure. Within the resolution of our XRD data, there is no clear stiffness change associated with the second structural reorganization at 14–16 GPa suggested by Raman spectra. However, x-ray absorption spectroscopy and extended x-ray absorption fine structure analyses of the compression behavior of a 6 nm anatase [27] suggested a transformation, on the scale of ~2 Å, of the nc anatase to an intermediate-range crystalline or TiO_2-II-like form at ~12 GPa and formation of the HDA-TiO_2 beginning at ~15 GPa. Thus, it appears that the kink in the P-V/V_o curve at 10–12 GPa (Fig. 3) signals the change to intermediate-range crystallinity. The nc anatase with intermediate crystallinity and the HDA form at $P > 15$ GPa appear indistinguishable from a stiffness perspective.

In summary, *in situ* angle-dispersive synchrotron XRD and Raman scattering data revealed an unusual compression behavior in nc anatase with a sharp increase in stiffness at 10–12 GPa. While the nanoscale TiO_2 has XRD and Raman signatures characteristic of *anatase* to ~27 GPa,

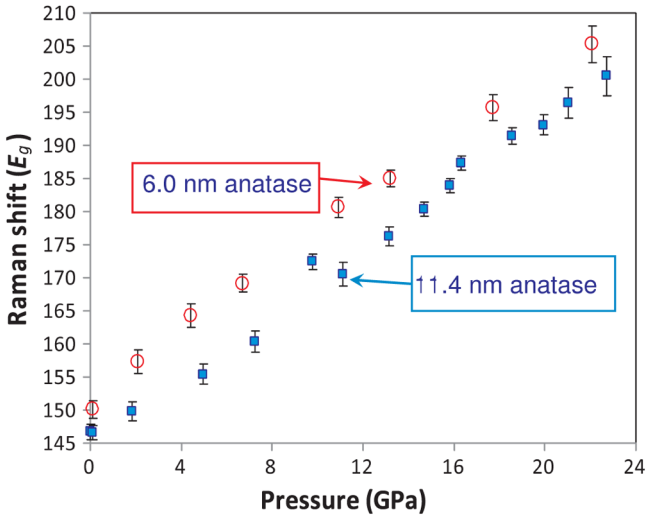

FIG. 5 (color online). The pressure shifts of the most intense E_g Raman band measured for the two nanocrystalline samples. Subtle breaks are seen at 10–12 and 14–16 GPa, more clear for the 11 nm anatase.

subtle local disorder on the scale of ~2 Å setting in under compression causes a drastic change in the stiffening behavior of the material at 10–12 GPa. This unique stiffening behavior represents the response of the structure, "seen" by both XRD and Raman scattering as anatase, to compression; however, this structure is significantly disordered at a scale of 2–3 Å. We suggest that similar nanomechanical behaviors may be encountered in other systems if investigated with multiple length scale probes.

GeoSoilEnviroCARS is supported by the National Science Foundation—Earth Sciences (EAR-0622171) and Department of Energy—Geosciences (DE-FG02-94ER14466). Use of the Advanced Photon Source is supported by the U.S. Department of Energy, Office of Science, Office of Basic Energy Sciences, under Contract No. DE-AC02-06CH11357. V. S. thanks the Australian Synchrotron Research Program for travel support.

*Corresponding author.
Varghese.Swamy@eng.monash.edu.au

[1] W. C. Oliver and G. M. Pharr, J. Mater. Res. **7**, 1564 (1992).
[2] O. Carp, C. L. Huisman, and A. Reller, Prog. Solid State Chem. **32**, 33 (2004).
[3] X. Chen and S. S. Mao, Chem. Rev. **107**, 2891 (2007).
[4] Q. Ye, P. Y. Liu, Z. F. Tang, and L. Zhai, Vacuum **81**, 627 (2007).
[5] J. Karch, R. Birringer, and H. Gleiter, Nature (London) **330**, 556 (1987).
[6] V. Swamy, L. S. Dubrovinsky, N. A. Dubrovinskaia, A. S. Simionovici, M. Drakapolous, V. Dmitriev, and H.-P. Weber, Solid State Commun. **125**, 111 (2003).
[7] V. Pischedda, G. R. Hearne, A. M. Dawe, and J. E. Lowther, Phys. Rev. Lett. **96**, 035509 (2006).
[8] E. Holbig, L. Dubrovinsky, G. Steinle-Neumann, V. Prakapenka, and V. Swamy, Z. Naturforsch. B, Chem. Sci. **61**, 1577 (2006).
[9] E. Holbig, L. Dubrovinsky, N. Miyajima, V. Swamy, R. Wirth, V. Prakapenka, and A. Kuznetsov, J. Phys. Chem. Solids **69**, 2230 (2008).
[10] S.-w. Park, J.-t. Jang, J. Cheon, H.-H. Lee, D. R. Lee, and Y. Lee, J. Phys. Chem. C **112**, 9627 (2008).
[11] V. Swamy, D. Menzies, B. C. Muddle, A. Kuznetsov, L. S. Dubrovinsky, Q. Dai, and V. Dmitriev, Appl. Phys. Lett. **88**, 243103 (2006).
[12] See EPAPS Document No. E-PRLTAO-103-057935 for details on materials and methods and additional supporting data documenting the break in the compression curve and hysteretic nature of the nc-anatase compression-decompression cycle. For more information on EPAPS, see http://www.aip.org/pubservs/epaps.html.
[13] A. Kern, A. A. Coelho, and R. W. Cheary, in *Diffraction Analysis of the Microstructure of Materials*, edited by E. J. Mittemeijer and P. Scardi (Springer, Berlin, 2004), p. 17.
[14] A. A. Coelho, TOPAS-Academic Users Manual, http://members.optusnet.com.au/~alancoelho/.
[15] Y. Fei, A. Ricolleau, M. Frank, K. Mibe, G. Shen, and V. Prakapenka, Proc. Natl. Acad. Sci. U.S.A. **104**, 9182 (2007).
[16] H. K. Mao, J. Xu, and P. M. Bell, J. Geophys. Res. B **91**, 4673 (1986).
[17] Q. F. Gu, G. Krauss, W. Steurer, F. Gramm, and A. Cervellino, Phys. Rev. Lett. **100**, 045502 (2008).
[18] T. Arlt, M. Bermejo, M. A. Blanco, L. Gerward, J. Z. Jiang, J. Staun Olsen, and J. M. Recio, Phys. Rev. B **61**, 14 414 (2000).
[19] S. Lundin, K. Catalli, J. Santillan, S.-H. Shim, V. B. Prakapenka, M. Kunz, and Y. Meng, Phys. Earth Planet. Inter. **168**, 97 (2008).
[20] I. E. Grey and N. C. Wilson, J. Solid State Chem. **180**, 670 (2007).
[21] X. Bokhimi, A. Morales, O. Novaro, T. Lopez, E. Sanchez, and R. Gomes, J. Mater. Res. **10**, 2788 (1995).
[22] I. Grey, I. Madsen, P. Bordet, N. Wilson, and C. Li, in *Advances in Ecomaterials*, edited by T. White, C. Ferraris, L. Yu, K. Halada, and O. Umezawa (Stallion Press, Singapore, 2005), Vol. 1, pp. 35–42.
[23] V. Swamy and L. S. Dubrovinsky, J. Phys. Chem. Solids **62**, 673 (2001).
[24] V. Swamy, A. Kuznetsov, L. S. Dubrovinsky, R. A. Caruso, D. G. Shchukin, and B. C. Muddle, Phys. Rev. B **71**, 184302 (2005).
[25] V. Swamy, A. Kuznetsov, L. S. Dubrovinsky, P. F. McMillan, V. B. Prakapenka, G. Shen, and B. C. Muddle, Phys. Rev. Lett. **96**, 135702 (2006).
[26] J. E. Lowther, High Press. Res. **26**, 131 (2006).
[27] A.-M. Flank, P. Lagarde, J.-P. Itie, A. Polian, and G. R. Herne, Phys. Rev. B **77**, 224112 (2008).
[28] J. R. Smyth, S. D. Jacobsen, and R. M. Hazen, Rev. Mineral. Geochem. **41**, 157 (2000).
[29] G. R. Hearne, J. Zhao, A. M. Dawe, V. Pischedda, M. Maaza, M. K. Nieuwoudt, P. Kibasomba, O. Nemraoui, J. D. Comins, and M. J. Witcomb, Phys. Rev. B **70**, 134102 (2004).
[30] T. Ohsaka, F. Izumi, and Y. Fujiki, J. Raman Spectrosc. **7**, 321 (1978).